ISIJ International, Vol. 59 (2019), No. 7, pp. 1323–1329

Relationship between Alloy Element and Weld Solidification Cracking Susceptibility of Austenitic Stainless Steel

Seidai UEDA,[1)] Kota KADOI,[2)]* Shun TOKITA[2)] and Hiroshige INOUE[2)]

1) Graduate School of Engineering, Osaka University, 11-1 Mihogaoka, Ibaraki, Osaka, 567-0047 Japan.
2) Joining and Welding Research Institute, Osaka University, 11-1 Mihogaoka, Ibaraki, Osaka, 567-0047 Japan.

(*Received on January 16, 2019; accepted on February 15, 2019; J-STAGE Advance published date: April 13, 2019*)

The effect of alloy elements such as niobium, titanium, and zirconium on the weld solidification cracking susceptibility in fully austenitic stainless steel was investigated. Niobium, titanium, or zirconium was added as an alloy element to Fe-24 mass%Cr-26 mass%Ni stainless steel. The cracking susceptibility was evaluated by crack length, number of cracks, and brittle temperature range (BTR) corresponding to results of the Trans-Varestraint test. Depending on the addition of the alloy element, the crack length increased; the length ordering tendencies between the total crack length (TCL) and the maximum crack length (MCL) differed with the alloy addition. The BTR was obtained by corresponding the MCL to the temperature range using the measured temperature history of the weld metal and was increased by the addition of the alloy element. The maximum BTR for the specimen with titanium was 266.9°C, which was three times that of the specimen without the alloy element. The MC carbide and the Laves phase formed at the dendrite cell boundaries as secondary phases. Solidification calculation based on the Scheil model was used to investigate the effect of the type of the alloy element on the solidification temperature range. Depending on the type of the alloy element, the solidification temperature range varied. A significant difference was found between the solidification temperature range and BTR in the case of the specimen with niobium.

KEY WORDS: solidification cracking; austenitic stainless steel; trans-varestraint test; segregation; brittle temperature range.

1. Introduction

Austenitic metals such as stainless steels and nickel-based alloys are highly susceptible to hot cracking such as solidification cracking during welding. Therefore, welding involving these metals is often avoided even though the metals have excellent properties such as a high corrosion resistance. It is known that the chemical composition, cooling rate, and constraint conditions are among the factors that influence cracking susceptibility.[1,2)] To improve cracking susceptibility, reduction in impurity elements such as phosphorous and sulfur and formation of the ferrite phase are often used.[3)] Impurity elements deteriorate cracking susceptibility because the segregation of the elements at the terminal of solidification corresponding to the low partition coefficient induces a drop in the solidus temperature. The formation of around 5% of the δ-ferrite phase by adjusting chemical composition (especially the ratio of chromium and nickel equivalents) can reduce this segregation because of the high solubility of the impurity elements in the δ-ferrite phase.[4)] However, it is impossible to form δ-ferrite in the case of fully austenitic materials such as the type 310S stainless steel and nickel-based alloy.

Besides, alloy elements of silicon, niobium, titanium and so on are also known to enhance cracking susceptibility owing to their low partition coefficients than that of the austenite phase.[5–8)] Niobium and titanium are often added to austenitic stainless steels and nickel-based alloys to modify weld decay (intergranular corrosion). On the other hand, the formation of MC carbide during solidification is known to improve cracking susceptibility.[7,9,10)] These elements trigger the formation of the MC-type carbide and the Laves phase as the secondary phase during solidification. The amount and morphology of the secondary phase depend on alloy elements. In addition, proper morphology and appropriate stoichiometric composition of the secondary phase can improve properties such as the solidification cracking susceptibility and corrosion resistance. However, the influence of the morphology of the secondary phase formations, namely, type, amount, combination of alloy elements, on these properties is still being studied. In the present study, the effect of the alloy element on the solidification cracking susceptibility and the secondary phase formation in fully austenitic stainless steels were investigated. The base composition of the specimen was Fe-24 mass% Cr-26 mass% Ni and 2 mass% of the alloy element of niobium, titanium, or zirconium was added. The relationship between the cracking susceptibility and the solidification sequence was examined by using the specimen with alloy elements.

* Corresponding author: E-mail: kadoi@jwri.osaka-u.ac.jp
DOI: https://doi.org/10.2355/isijinternational.ISIJINT-2019-035

2. Experimental Procedure

2.1. Material and Specimen Fabrication

Table 1 shows chemical compositions of the specimens used. Fe-24%Cr-26%Ni (24Cr-26Ni) stainless steels with niobium, titanium or zirconium were employed. The amount of the alloy elements was set at 2.0%. The specimens were fabricated through vacuum induction melting and hot rolling. The specimen geometry was $100^{W} \times 50^{L} \times 5^{t}$ mm. The chemical compositions were measured with an optical emission spectrometer. Hereafter, the base composition of Fe-24%Cr-26%Ni is called 24Cr-26Ni for simplicity. In addition, the specimens with 2% alloy element added to the base composition are called 2Nb, 2Ti, and 2Zr.

2.2. Evaluation of the Solidification Cracking Susceptibility

The Trans-Varestraint test was used for the evaluation of the solidification cracking susceptibility. Gas tungsten arc welding was carried out under the welding speed of 0.1 m/min, arc current of 120 A, and arc length of 2 mm. When the trailing edge of the molten pool moved to the centre of the specimen, the bending strain was loaded on the specimen surface and the welding stopped. The augment strain was 4.1%, which was sufficient for saturated to open the cracks.[11,12]

After the test, the crack length was measured by using a scanning electron microscope (SEM). As shown in **Fig. 1**, the crack length was measured in the normal direction from the liquid/solid boundary at the crack initiation point for each crack. The number of cracks, total crack length (TCL), and maximum crack length (MCL) were derived as evaluation indexes of the solidification cracking susceptibility. The temperature history was measured by inserting a thermocouple into the backside of the molten pool during welding. The maximum crack length was converted into the brittle temperature range (BTR) by using the temperature history.

The cross-sectional microstructures of the specimens were analysed through an optical microscope (OM) and SEM. Microfocus X-ray diffraction (XRD) analyses were conducted to identify the secondary phases. The specimens were prepared by electrochemical etching with 10% oxalic acid after final polishing with colloidal silica. Furthermore, energy dispersive X-ray spectrometry (EDX) with transmission electron microscopy (TEM) was carried out to investigate the chemical distributions of secondary phases. The TEM specimens were prepared by using the carbon extraction replica method.[13]

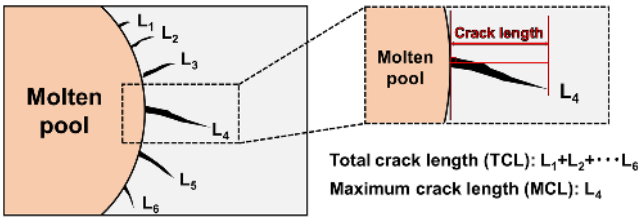

Fig. 1. Schematic of measurement method of cracks. (Online version in color.)

2.3. Solidification Calculation

Solidification cracking is induced by shrinkage strain during the solidification sequence. Therefore, the solidification temperature range ΔT, which is the temperature difference between the liquidus T_L and solidus T_S temperatures, is one of the important factors to evaluate the solidification cracking susceptibility. Hence, solidification calculation based on the Scheil model was used to investigate the effect of the type of alloy element on ΔT. Thermo-Calc software (version: 2017b, database: TCFE7) was used for calculations. In this study, T_L was considered as the temperature of the solidification start and T_S was considered as the temperature of the solid fraction of 95%.[5,14] The ΔT was calculated from the difference between T_L and T_S in the calculation. Chromium, nickel, carbon, niobium, and titanium were considered in the calculation. The MC carbide and the Laves phase predicted to form during solidification were set as the secondary phase. However, the calculation did not converge for 2Zr. Therefore, solidification calculation was not carried out for 2Zr. The miscibility gap was set on the FCC A_1 phase to distinguish the formation of austenite and the MC carbide.

3. Result and Discussion

3.1. Crack Distribution and Length

Figure 2 presents the crack distribution in 2Zr after the Trans-Varestraint test. Long cracks can be observed around the centre of the trailing edge of the molten pool. The same tendency is observed for all specimens. On the other hand, the crack distributions, namely, the length and number of cracks, are different depending on the type of the alloy element.

The TCL and MCL of each specimen are given in **Fig. 3**. Both TCL and MCL increase when the alloy element is added. The TCLs are 9.01 mm in 24Cr-26Ni, 12.48 mm in 2Nb, 10.52 mm in 2Ti, and 10.22 mm in 2Zr. The TCL decreases in the 2Nb>2Ti>2Zr order. The MCL in 24Cr-26Ni is 0.68 mm. The maximum MLA value is 1.97 mm in 2Ti, which is about three times compared with the MCL in 24Cr-26Ni. The MCL decreases in the 2Ti>2Zr>2Nb order.

Table 1. Chemical compositions of specimens (mass%).

	C	Si	Mn	P	S	Cr	Ni	Nb	Ti	Zr	Fe
24Cr-26Ni	0.046	0.54	0.87	0.025	0.0012	23.20	26.50	–	–	–	Bal.
2Nb	0.044	0.51	0.83	0.029	0.0015	23.50	26.30	2.13	–	–	Bal.
2Ti	0.036	0.53	0.80	0.023	0.0013	23.80	26.50	–	1.97	–	Bal.
2Zr	0.046	0.53	0.81	0.027	0.0012	24.10	27.50	–	–	1.99	Bal.

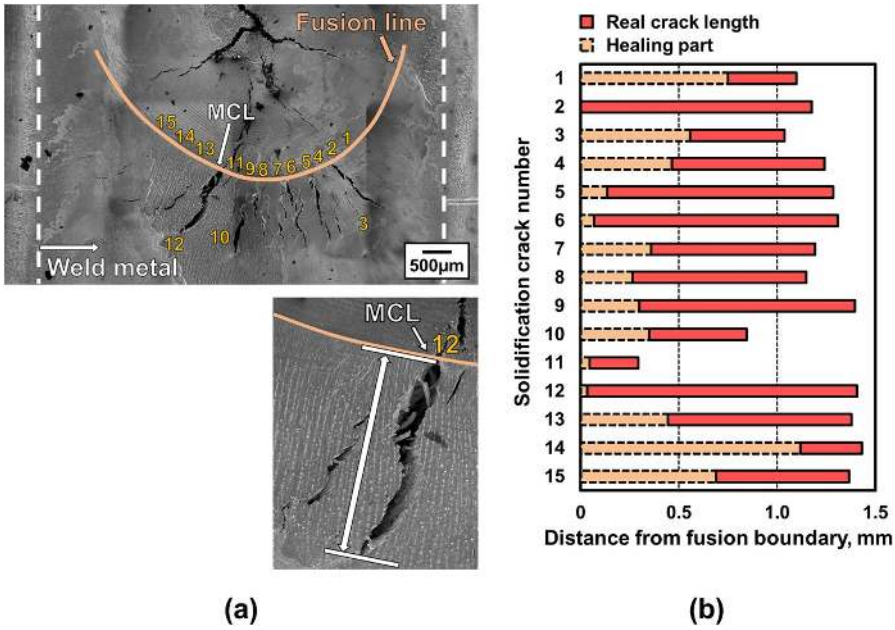

Fig. 2. Crack distribution of specimen of 2Zr. a) Surface of 2Zr after Trans-Varestraint test. b) Crack length of solidification cracks. (Online version in color.)

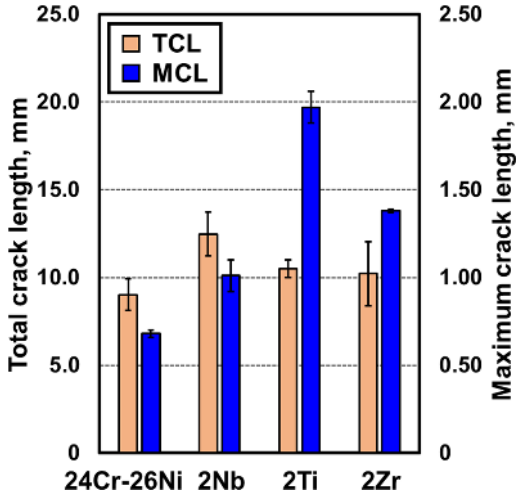

Fig. 3. TCL and MCL of each specimen. (Online version in color.)

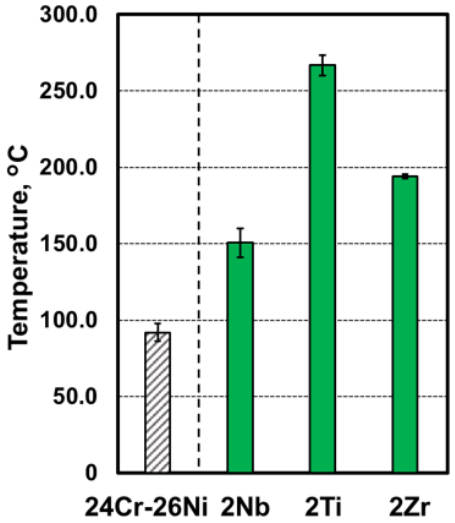

Fig. 4. BTR of each specimen. (Online version in color.)

Until now, both TCL and MCL have been applied as indexes for the evaluation of the solidification cracking susceptibility. However, there are different tendencies of the order of the lengths between TCL and MCL. Furthermore, an average 22 cracks of approximately 1 mm occur in the 2Nb case. On the other hand, in the 2Ti case, an average 7.5 cracks of approximately 2 mm occur. The average grain size in the weld metal of each specimen was nearly the same, even though the grain size is known to influence susceptibility.[15] Therefore, it is thought that the type of alloy element influences the length and number of cracks. Hence, it is difficult to directly evaluate cracking susceptibility with only the TCL and MCL. Most of the solidification cracks in the weld metal occur at its centre along the weld line direction. In the case of the Trans-Varestraint test, long solidification cracks tend to occur at the centre of the backside of the molten pool because the bending at the centre becomes high. Besides, sufficient bending strain can open the solidification crack to the maximum.[12] On the other hand, it is difficult to control the number and the position of crack(s) which affect the TCL. Therefore, MCL and BTR must be recommended as indexes for the evaluation of the solidification cracking susceptibility in the Trans-Varestraint test.

Figure 4 shows the BTR of each specimen obtained by converting from the MCL into the temperature range using the measured temperature history of the weld metal. The BTR in 24Cr-26Ni shows 92.0°C. This value is almost the same as the BTR in the type 310S stainless steel, which is generally used as fully austenitic stainless steel.[16] The BTR of 2Ti is 266.9°C, 2Nb is 150.1°C, and 2Zr is 194.1°C. The value of 2Ti is the highest and approximately three times that of 24Cr-26Ni. The influence of the alloy element on the increment of BTR is different. Because the BTR is increased approximately by 170°C by adding titanium, it is assumed that titanium significantly influences the solidification cracking susceptibility.

3.2. Microstructure in Weld Metal

Cross sections of microstructures in the weld metal of each specimen are shown in **Fig. 5**. In each specimen, the austenite phase is found as the primary phase. Whereas 24Cr-26Ni is single phase solidification of austenite, secondary phases are found at the dendrite cell boundaries in 2Nb, 2Ti, and 2Zr. Each alloy element was detected from the secondary phases in each specimen through the EDX analysis. Both granular and film-like constituents are observed in 2Nb. The granular constituent is mainly formed in 2Ti. Film constituents along dendrite can be observed in 2Zr. The XRD analysis revealed that the constituents were the MC carbide and the Laves phase in the specimens. The alloy elements are segregated between the dendrite cell boundaries owing to a low partition coefficient than that of the austenite phase. Therefore, the secondary phase must be formed owing to the enrichment of alloy elements between the dendrite cell boundaries because of segregation.

Figure 6 shows the bright-field image of TEM and area mappings of the alloy element near the constituent in each specimen. Each alloy element is enriched in the secondary phase. Carbon is enriched at the constituents indicated by the solid arrow in the bright-field image of Fig. 6, and chromium, nickel, and iron are enriched at the constituents indicated by the open arrow in the bright-field image of Fig. 6. Therefore, in the case of 2Nb, as shown in Fig. 6(a), NbC as the MC carbide and the Laves phase consisting of chromium, nickel, or iron with niobium is formed. In addition, as shown in Fig. 6(b), the Laves phase consisting of chromium, nickel, or iron with titanium is formed in 2Ti. In the case of 2Zr, as shown in Fig. 6(c), ZrC as the MC carbide and the Laves phase consisting of chromium, nickel, or iron with zirconium is formed in 2Zr. According to the geometry of the constituents observed with TEM, the MC carbide tends to be film-like and the Laves phase is granular. Similar tendencies are also confirmed in 2Nb and 2Ti. According to the microstructure as shown in Fig. 5, in the case of 2Nb, it is considered that the ratio of the MC carbide and the Laves phase is the same because the amounts of the granular and the film-like constituents are nearly the same. The Laves phase must be formed in 2Ti and the MC carbide in 2Zr because of their mainly granular and film-like constituents, respectively.

3.3. Solidification Calculation

The relation between ΔT and BTR was investigated. The results of the solidification calculation based on the Scheil model are presented in **Fig. 7**. In the case of 2Nb shown in Fig. 7(a), the inflection point is found at 1 067.2°C. This point indicates the start temperature of the formation of the Laves phase. On the other hand, in the case of 2Ti, the first inflection point is found at 1 318.9°C and the second one appears at 1 103.0°C. The first inflection point is the start temperature of the formation of MC carbide and the second one is the start temperature of the formation of the Laves phase. Depending on the type of the alloy element, the number of the inflection points and the start temperature of the secondary phase formation are different. It is suggested that these differences are influenced by the partition coefficient of the alloy element, Gibbs energy of the formation of the secondary phase, and the activity of alloy elements and carbon.

A comparison between ΔT and BTR is shown in **Fig. 8**. It is known that there is correlation between ΔT and BTR.[5] In the case of 24Cr-26Ni, ΔT is 70.1°C, and there is no significant difference between ΔT and BTR. Depending on the addition of alloy elements, ΔT and BTR have nearly the same values in the case of 2Ti. However, in the case of 2Nb, ΔT is 359.4°C; and the difference is around 200°C with BTR. Whereas both the MC carbide and the Laves phase were found in 2Nb, only the Laves phase was formed in the solidification calculation. In the solidification calculation in these chemical compositions, the amount of segregation of alloy elements such as niobium and titanium is significant and larger than the recommended value in the database. It is assumed that the lack of the reliability of database owing to the segregation amount above the recommended value and the ΔG_0 of niobium larger than that of titanium according to the Ellingham diagram[17] influence the differences in the secondary phase formation between the solidification calculation and actual solidification, namely, the difference between ΔT and BTR. Therefore, it is necessary to use a database that corresponds to the chemical composition of the specimen used and construct a more detailed calculation model. In addition, it is also assumed that segregation of excess alloy elements during solidification influences this difference.

3.4. Effect of Alloy Element on Solidification Cracking Susceptibility

The experimental results show that the tendency of BTR is different and depends on the type of alloy element, and the addition of titanium induces a high BTR. According to the Ellingham diagram, zirconium and titanium are easier to form the MC carbide than niobium.[17] Furthermore, the atomic weight of titanium is approximately half that of niobium or zirconium. As shown in section 3.2, both the MC carbide and the Laves phase are observed in the weld metals in each specimen. However, the type and the amount of the formed secondary phase depend on the type of the alloy element. The MC carbide and the Laves phase were formed at the same ratio in 2Nb. In contrast, the Laves phase

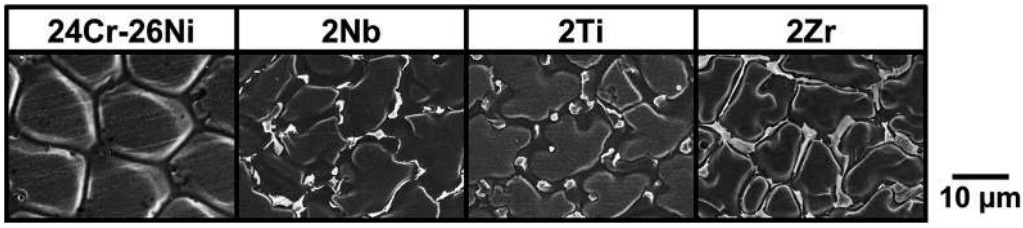

Fig. 5. Cross sections of microstructures of each specimen.

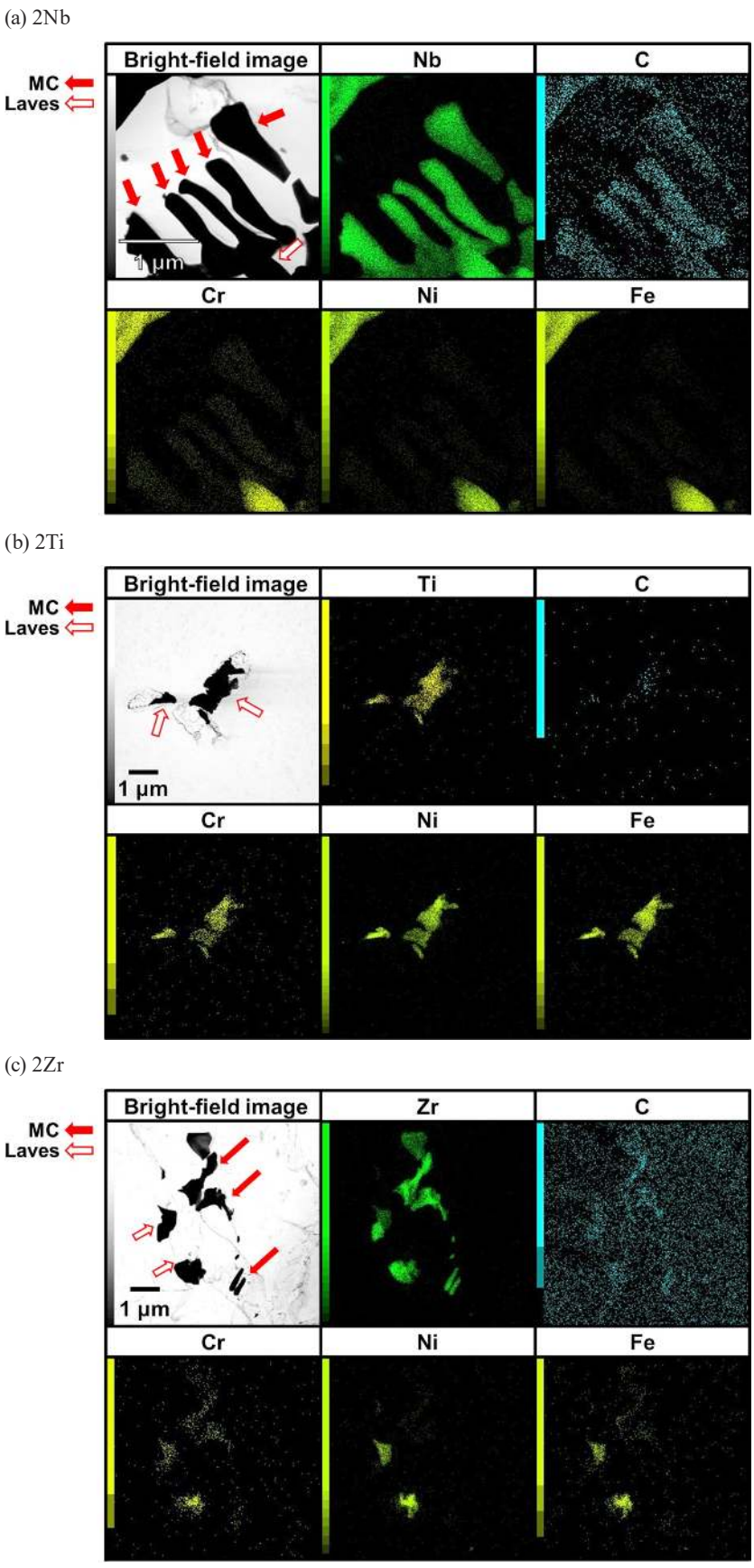

Fig. 6. TEM-EDX mapping analysis of secondary phase in each specimen. (Online version in color.)

mainly formed in 2Ti, and the MC carbide formed in 2Zr. The calculation results showed that the MC carbide and the Laves phase formed during solidification in 2Ti. Besides, the ΔT of 2Ti was smaller than that of 2Nb, and the start temperature of the MC phase as the secondary phase was higher than that of the Laves phase. However, the BTR of 2Ti was 100°C higher than that of 2Nb, and the formation amount of the MC carbide in 2Ti is much smaller than that

of 2Nb or 2Zr.

It is known that the MC carbide should form by segregation of the alloy element during solidification and the Laves phase forms during solidification and precipitates at the solid state. Therefore, the Laves phase observed in this study should be not only formed during the solidification but also precipitated at the solid state. This should cause the segregation of titanium in the residual liquid phase up to a low temperature. According to the quenched microstructure observed, as shown in **Fig. 9**, the Laves phase of the granular constituent, which is found in the microstructure at room temperature, is observed from the low temperature side of solidification. Furthermore, the granular constituent of 2Ti is found from the lower temperature side as compared with 2Nb and 2Zr. Therefore, it is predicted that a lot of liquid phase remained until a low temperature. Therefore, it is considered that BTR in 2Ti expands. The amount of the excess titanium segregated must be more than that of niobium or zirconium because of the difference in their atomic weights. Thus, the reduction in the solidus temperature, depending on the segregation of the excess titanium, induces an increase in the BTR of 2Ti. On the other hand, even though zirconium has higher affinity for carbide compared to that for niobium, the BTR of 2Zr is larger than that of 2Nb. Although it is assumed that the partition coefficient of the alloy element

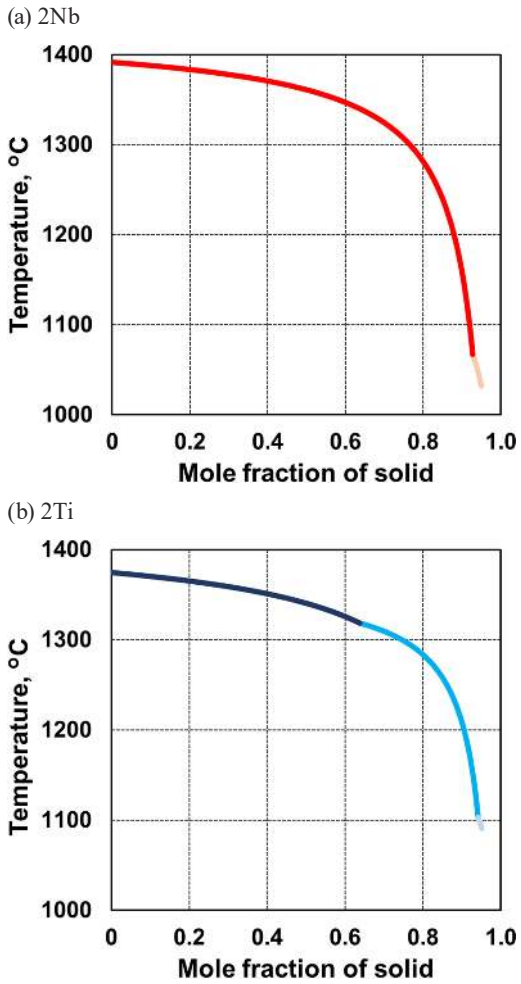

Fig. 7. Solidification calculations based on Scheil model. (Online version in color.)

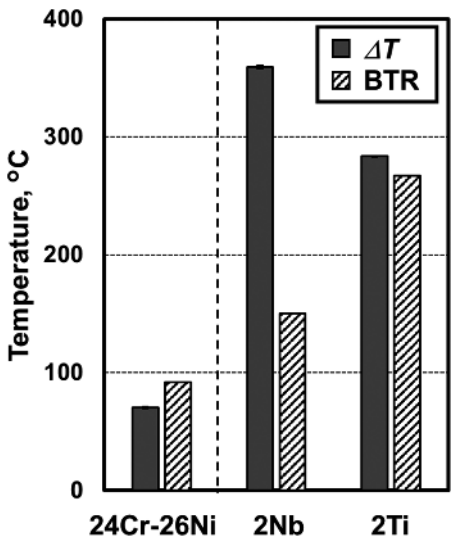

Fig. 8. Comparison between ΔT and BTR.

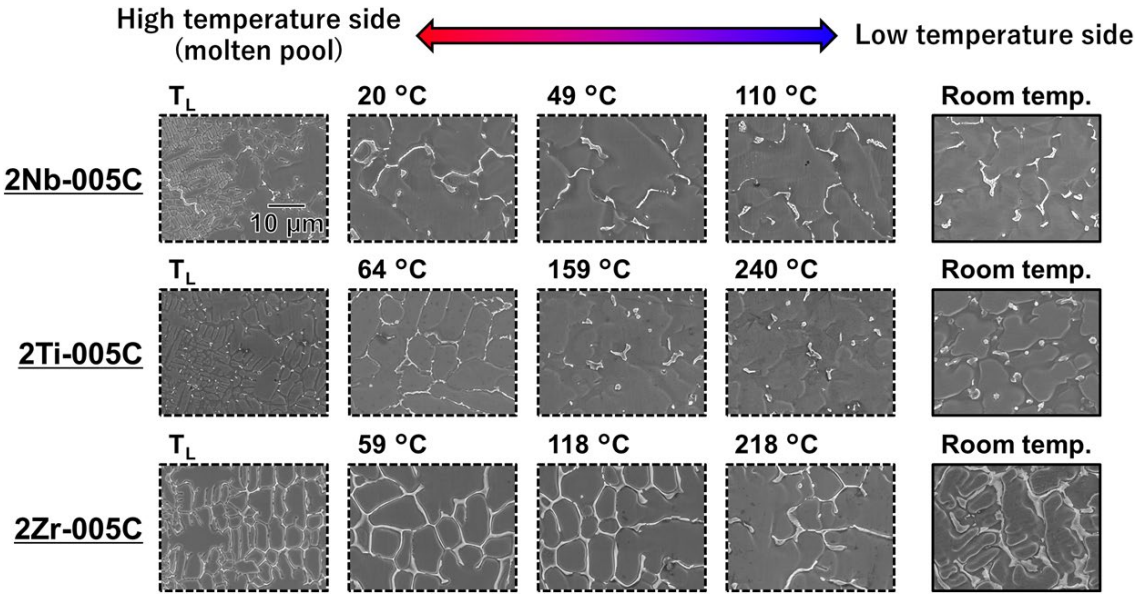

Fig. 9. Quenched microstructure in weld metal of each specimen. (Online version in color.)

influences the tendency of the BTR, the details of this factor are still unclear. Hence, it is necessary to investigate the tendency of segregation in detail depending on the addition of the alloy elements and construct a more detailed calculation model that takes segregation into account.

4. Conclusions

The effect of alloy elements such as niobium, titanium, or zirconium on the weld solidification cracking susceptibility in fully austenitic stainless steel was investigated. The TCL decreased in the 2Nb>2Ti>2Zr order. On the other hand, the MCL decreased in the 2Ti>2Zr>2Nb order. The tendencies for the ordering of the lengths between the TCL and the MCL were different. The BTR decreased in the 2Ti>2Zr>2Nb order. The maximum BTR of 266.9°C in 2Ti was approximately three times that in 24Cr-26Ni. The secondary phases such as the MC carbide and the Laves phase were formed at the dendrite cell boundaries in the specimens containing alloy elements. The MC carbide and the Laves phase were formed in the same ratio in 2Nb. In contrast, the Laves phase mainly formed in 2Ti and the MC carbide formed in 2Zr. The calculated ΔT and BTR nearly had the same values in the case of 2Ti. However, the ΔT in 2Nb was 359.4°C, and the difference was around 200°C with BTR in 2Nb. Whereas both the MC carbide and the Laves phase were found in the microstructure of 2Nb, only the Laves phase was formed in the solidification calculation. It is thought that the difference between the solidification calculation and actual solidification, depending on the segregation of the excess alloy elements during solidification, influences the difference between the ΔT and the BTR. It is necessary to investigate the tendency of segregation in detail depending on the addition of the alloy elements and construct a more detailed calculation model that takes segregation into account.

REFERENCES

1) S. Kou: Welding Metallurgy, John Wiley & Sons, Hoboken, NJ, (2003), 263.
2) J. N. DuPont, J. C. Lippold and S. D. Kiser: Welding Metallurgy and Weldability of Nickel-Base Alloys, John Wiley & Sons, Hoboken, NJ, (2009), 208.
3) L. Li and R. W. Messler, Jr.: *Weld. J.*, **78** (1999), 387.
4) V. Kujanpaa, N. Suutala, T. Takalo and T. Moisio: *Weld. Res. Int.*, **9** (1979), 55.
5) K. Kadoi and K. Shinozaki: *Metall. Mater. Trans. A*, **48** (2017), 5860.
6) Y. Arata, F. Matsuda and S. Katayama: *Trans. JWRI*, **6** (1977), 105.
7) T. Ogawa and E. Tsunetomi: *Weld. J.*, **61** (1982), 82.
8) V. Shankar, T. P. S. Gill, A. L. E. Terrance, S. L. Mannan and S. Sundaresan: *Metall. Mater. Trans. A*, **31** (2000), 3109.
9) J. N. Dupont, C. V. Robino and A. R. Marder: *Weld. J.*, **77** (1998), 417.
10) H. Hirata, K. Ogawa, S. Hongou, T. Kumagai, T. Yamakawa, S. Koga and K. Nishimoto: *Q. J. Jpn. Weld. Soc.*, **19** (2001), 680 (in Japanese).
11) J. N. DuPont, J. R. Michael and B. D. Newbury: *Weld. J.*, **78** (1999), 408.
12) D. Wang, S. Sakoda, K. Kadoi, K. Shinozaki and M. Yamamoto: *Q. J. Jpn. Weld. Soc.*, **33** (2015), 39 (in Japanese).
13) T. Akutagawa, I. Uchiyama and A. Fukami: *Tetsu-to-Hagané*, **43** (1957), 1222 (in Japanese).
14) T. Ogura, S. Ichikawa and K. Saida: *Weld. Int.*, **32** (2018), 436.
15) K. Shinozaki, P. Wen, M. Yamamoto, K. Kadoi, Y. Kohno and T. Komori: *Q. J. Jpn. Weld. Soc.*, **29** (2011), 90 (in Japanese).
16) D. Wang, K. Kadoi, K. Shinozaki and M. Yamamoto: *ISIJ Int.*, **56** (2016), 2022.
17) S. R. Shatyski: *Oxid. Met.*, **13** (1979), 105.